

Constraint-Aware Feature Learning for Parametric Point Cloud

Xi Cheng Ruiqi Lei Di Huang Zhichao Liao Fengyuan Piao Yan Chen
Pingfa Feng Long Zeng[†]

Tsinghua Shenzhen International Graduate School, Tsinghua University, Shenzhen, China

{chengxi23, leirq22}@mails.tsinghua.edu.cn, dihuangdylan@gmail.com,

{liaozc23, pfy22, chenyan23}@mails.tsinghua.edu.cn,

fengpff@tsinghua.edu.cn, zenglong@sz.tsinghua.edu.cn

Abstract

Parametric point clouds are sampled from CAD shapes and are becoming increasingly common in industrial manufacturing. Most existing CAD-specific deep learning methods only focus on geometric features, while overlooking constraints which are inherent and important in CAD shapes. This limits their ability to discern CAD shapes with similar appearance but different constraints. To tackle this challenge, we first analyze the constraint importance via a simple validation experiment. Then, we introduce a deep learning-friendly constraints representation with three vectorized components, and design a constraint-aware feature learning network (CstNet), which includes two stages. Stage 1 extracts constraint feature from B-Rep data or point cloud based on shape local information. It enables better generalization ability to unseen dataset after model pre-training. Stage 2 employs attention layers to adaptively adjust the weights of three constraints' components. It facilitates the effective utilization of constraints. In addition, we built the first multi-modal parametric-purpose dataset, i.e. Param20K, comprising about 20K shape instances of 75 classes. On this dataset, we performed the classification and rotation robustness experiments, and CstNet achieved 3.52% and 26.17% absolute improvements in instance accuracy over the state-of-the-art methods, respectively. To the best of our knowledge, CstNet is the first constraint-aware deep learning method tailored for parametric point cloud analysis in CAD domain. Our project page with source code is available at: <https://cstnetwork.github.io/>.

1. Introduction

Parametric point clouds are sampled from CAD shape instances or captured from various industrial scenarios by common digital devices. As illustrated in Fig. 1, CAD shape

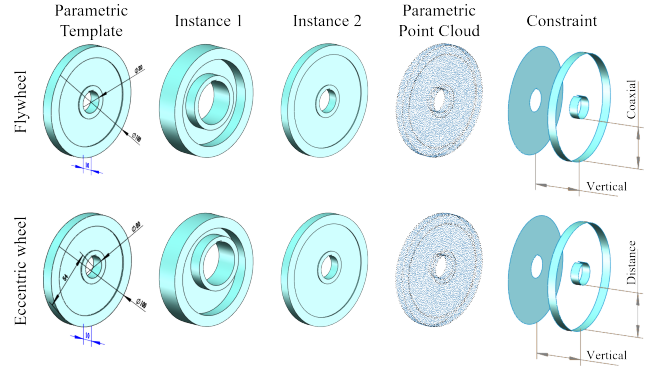


Figure 1. **Motivation.** Some CAD shapes are visually similar but serve different functions. The eccentric wheel has a distance constraint, i.e. its rotation axis is offset from outer cylindrical surface. It is used for precise positioning or tension adjustment. In contrast, the flywheel has a coaxial constraint, i.e. its rotation axis is coaxial with outer cylindrical surface. It is used to store rotational kinetic energy. While these shapes are challenging to distinguish visually, they can be effectively differentiated from constraints.

instances are typically instantiated from parametric templates, which comprise primitives, constraints, and shape parameters. By specifying a series of parameter configurations, a template can be instantiated into a family of CAD shape instances [62]. In industrial domain, many CAD shapes are visual similar but have different constraints in their functional regions. This poses challenges for existing point cloud deep learning methods which based on geometric features only. Thus, a constraint-aware feature learning method for parametric point cloud is fundamental for a wide range of industrial applications, such as engineering model design and product manufacturing.

First, most existing studies [26, 41, 58, 65] focus on primitive regularity (e.g. uniform appearance and distinct boundaries). They usually leverage geometric features only, but ignore those constraints between primitives. Although these methods have been effectively applied in point cloud

segmentation and primitive reconstruction, they inherently limit their discrimination capability for CAD shapes that are visually similar yet functionally distinct. While some studies discussed constraints in 2D engineering sketches [8, 40], the considered primitives in 2D sketches are supposed available and generally few in number. Thus, these approaches can be hardly extended to 3D parametric point clouds. Second, most CAD-specific methods rely on specialized datasets with additional labels (*e.g.* primitive, parameter, and normal labels). However, point clouds are typically acquired via LiDAR or RGB-D cameras, and in most cases only contain coordinate information. It thus restricts the practical applicability of these approaches. Third, there are still numerous challenges in constraint-aware point cloud analysis. Constraints represent the spatial relationships between primitives, but the number and types of primitives cannot be directly obtained from point clouds. Predicting primitives from point clouds also poses challenges. The unordered nature of point clouds results in unordered outcomes, leading to a mismatch between the predicted primitives and those in the constraint labels. In addition, processing relations between every pair of primitives would produce an overwhelming amount of data, since some CAD shapes contain many primitives. Assuming that the constraints have been obtained, effectively leveraging them remains a significant challenge.

To address the aforementioned issues, we transform the traditional constraint representation (*e.g.* constraints in SolidWorks or UG [3]) into three vectorized sub-features: primitive’s Main Axis Direction (MAD), Adjacency (Adj), and Primitive Type (PT). Given the completeness of traditional constraint representation, these three sub-features can effectively capture constraints. Representing constraints with MAD, Adj, PT converts the relations between primitive pairs into relations between primitives and a common reference, thereby significantly reducing the total number of relations. Moreover, the MAD, Adj, PT can be inferred by local point patches, and the local features of CAD shapes are predominantly composed of primitives such as planes and cylinders. Consequently, a model that relies solely on local features can generalize to unseen datasets after pre-trained, this property eliminates the reliance on constraint labels during practical applications. To mitigate the impact of point cloud unordered nature, we encode MAD, Adj, PT as point-wise features. As a result, each point with constraints in point cloud is represented as (X, Y, Z, MAD, Adj, PT). The aforementioned processing transform the constraints into deep learning-friendly form. After that, we designed the constraint prediction from point cloud (CstPnt) module to obtain MAD, Adj, PT. The CstPnt module is based solely on local features, experiments show that it exhibits strong generalization ability on unseen datasets, and its training data can be easily obtained by processing

unlabeled B-Rep data. Following constraint acquisition, we separately extract features from MAD, Adj, PT, and apply attention mechanism to weight these features, thereby facilitating their effective utilization.

We quantitatively evaluate CstNet on ABC [20] and Param20K dataset: constraints prediction, classification, and rotation robustness evaluation. For constraints prediction, our CstPnt module (in CstNet Stage 1) surpasses the state-of-the-art (SOTA) by around 5% and 14% instance accuracy in ABC (test set) and Param20K (unseen dataset), respectively. For classification and rotation robustness on Param20K, CstNet outperforms the SOTA by 3.52% and 26.17% instance accuracy, respectively.

In summary, our contributions are threefold:

- We introduced a deep learning-friendly vectorized representation and designed the first constraint-aware feature learning network CstNet for effective constraint acquisition and leveraging for parametric point cloud.
- We built the first parametric-purpose Param20K dataset, which consists of about 20K shape instances of 75 classes. Each instance include mesh, point cloud, and B-Rep data. Given the current scarcity of labeled CAD shape datasets, Param20K offers a solid basis for future studies in parametric CAD domains.
- We conducted extensive experiments on constraint acquisition, classification, robustness evaluation and ablation studies. The performance of CstNet has a significant improvement compared with SOTA methods which usually focus on geometric data only.

2. Related Work

General point cloud analysis. View-based methods typically project the point cloud from multiple views, the obtained figures are then fed in convolutional neural networks (CNNs) for feature extraction [7, 17, 42, 47, 59, 60]. How to address information loss during the projection and optimizing viewpoints play a critical role. Voxelization-based methods convert point clouds into 3D voxels, and then employ 3D CNNs for feature extraction [19, 22, 33, 39, 45, 52]. The size and orientation of 3D voxels significantly influences the accuracy of these methods, and information loss occurs during the conversion to voxels. Point-based methods directly use points as input, thereby avoiding information loss associated with view-based and voxel-based methods, it is also the most popular point cloud learning method [2, 5, 9, 11, 12, 27, 29–31, 36–38, 43, 46, 51, 53–55, 57, 63, 64, 66]. The unordered nature and rotational invariance of point clouds make it challenging to employ methods similar to traditional CNNs for feature extraction, and kNN is a commonly adopted approach.

Parametric point cloud analysis. The most extensive application of these methods lies in segmentation and primitive fitting [26, 41, 58, 65]. CAD shapes are typically com-

posed of regular primitives, such as plane, cylinder, cone, and the variety of such elements is limited. Therefore, leveraging primitives' distinct shape features enables these methods to achieve superior segmentation and primitive fitting outcomes compared to general approaches. These methods generally predicting primitives parameters, and subsequently fed into downstream modules, these modules may incorporate specific primitive fitting algorithms. Despite their superior ability to exploit the shape features of individual primitives, these methods overlooked the constraints between primitives. This oversight limited their ability to distinguish CAD shapes that share similar appearances but serve different functions. Moreover, the primitive parameters predicting procedure necessitates the corresponding parameter labels. In practical, when sampling point clouds from CAD shapes, only coordinates can be obtained in most cases, which limits the applicability of these methods.

Other CAD-specific studies. B-Rep-based methods typically involve B-Rep data conversion and feature extraction, the challenge lies in converting B-Rep into deep learning compatible format. These approaches are commonly applied to classification [15], segmentation [6, 21], assembly [16, 48], engineering sketch generation [13], and CAD operation sequence prediction [50, 67]. Mesh-based learning methods use triangle models as input, such as STL and OBJ, contributions often rely on mechanical datasets provided by the authors. These methods are primarily used for classification [32], retrieval [4], segmentation [44], and B-Rep generation [10]. Sketch-based learning takes hand-drawn sketches as input, with outputs typically being engineering sketches [10, 28, 34, 40, 49], 3D models [23, 24, 62], or CAD operation sequences [56]. A key challenge is incorporating the regularity and connectivity of primitives, which is typically overlooked in graphic object analysis.

While there has been substantial progress in CAD-specific studies, further innovation on constraint learning is demanded to ensure higher accuracy and robustness.

3. Method

3.1. Is Constraint Important?

We aim to utilize constraints to distinguish visually similar but functionally distinct CAD shapes. To answer whether constraints could enhance deep learning methods' performance, we designed the following validation experiments. The objective is to compare the prisms shown in Fig. 2 with cuboids. In each experiment, only prisms with a specific angle are selected, creating a binary classification task between prisms and cuboids. Consequently, eight independent experiments are conducted to cover all angles. As the prism's angle approaches 90° , its resemblance to cuboids increases, making it progressively more challenging to distinguish them. The constraint-aware model is built on

PointNet++ backbone, which predicts constraints and then adopts it for classification. The constraints are represented as the relation between the point attached primitive and a reference plane, more details in supplementary.

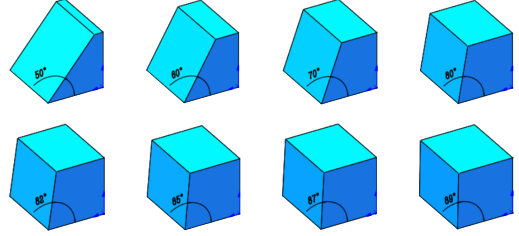


Figure 2. Prisms compared to cuboid.

From results presented in Fig. 3, for prisms with angles from 50° to 87° , incorporating constraints improves classification accuracy significantly, while the 89° prisms are too similar to the cuboids, all methods cannot distinguish them.

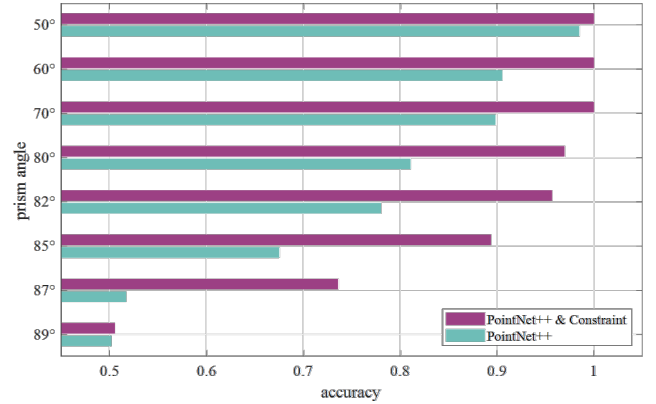


Figure 3. Classification accuracy of validation experiments.

However, the constraint learning method designed in the validation experiments is only applicable to simple scenarios. To develop a more generalized approach, we further investigated the constraint representation and deep learning architecture tailored for parametric point clouds.

3.2. Constraint Representation

In general, constraints should be defined as point-wise attribute for point clouds, analogous to normal vector. As point cloud is inherently unordered, assigning constraints at the point-wise level ensures that their representation is independent of point permutation. Following the constraint definitions in CAD software is not applicable. However, once the constraint is applied, the positional relations between primitives become fixed. Therefore, if the type of primitives and their relations are determined, the constraints on CAD shapes can be defined comprehensively.

The point-wise primitive type can be represented as the type of the primitive to which the point is attached, using

one-hot encoding. The positional relation is defined as the combination of main axis direction and adjacency. Considering that the direction of primitives' main axis is unique, as shown in Fig. 4, relations such as parallel and vertical could be derived from the direction of their main axes. However, some dimensional relations can not, such as the cylinders' radius equivalence. Thus, additional data is required to supplement this information. Since the connected primitives are the basis of CAD shapes, the adjacency and main axis direction impose limitations on the distance and size of primitives. For example, in a cuboid, the adjacency and normal of the six faces ensure that the distance between the top and bottom faces equals the height of the front face, and the size of the back face is the same as the front one. Therefore, if the adjacency is combined with main axis directions, the positional relation can be determined comprehensively. Adjacency represents the connection between primitives and cannot be expressed as point-wise attribute directly. The edges are key indicators of adjacency, with each edge corresponding to two adjacent primitives, adjacency can therefore be inferred from edges. For point cloud, an edge can be represented by marking points near it, thus, point-wise adjacency is expressed as whether the point is near an edge, which can be represented by two-channel one-hot vector. In summary, each composition of constraints in parametric point cloud is illustrated in Fig. 5, and each point with constraint is expressed as (X, Y, Z, MAD, Adj, PT) .

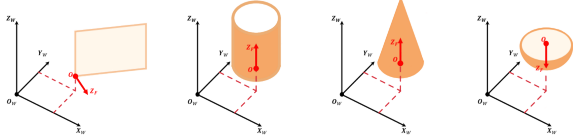


Figure 4. **Main Axis Direction of primitives.** Plane: normal vector. Cylinder, cone, sphere: rotation axis. Main Axis Direction requires unique process, details are provided in Supplementary.

We represent constraints by MAD, Adj, PT, is this approach sufficient to handle most constraints? For PT, commercial CAD systems typically classify primitives into plan, cylinder, cone, sphere, and free-form surface. Among these, plane, cylinder, and cone are primarily influenced by constraints, while spherical and free-form surfaces rely heavily on their geometric features. Therefore, considering plane, cylinder, and cone is sufficient for constraint representation. For sphere and free-form surface, the Stage 2 of CstNet also incorporate geometric features (feed in coordinates). MAD correspond to directional constraints (*e.g.* parallel and vertical), and MAD combined with PT represent dimensional constraints (*e.g.* distance and tangent). Through MAD and Adj, most common constraint types can be covered. Therefore, the combination of MAD, Adj, and PT is sufficient to represent the majority of constraints.

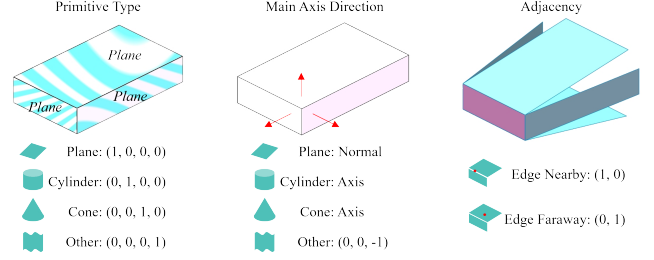


Figure 5. **Constraint representation of parametric point cloud.**

3.3. Constraint Acquisition

The Stage 1 of CstNet is designed to obtain constraints, as shown in the left of Fig. 7. When B-Rep data is available, the constraint computation from B-Rep (CstBRep) module is developed to obtain constraints. For the input B-Rep data, tessellation is performed by OCCT to generate a mesh model, followed by Poisson disk sampling [25] via pymeshlab to ensure a uniform point distribution and control the point count, if point cloud generation is not needed, this step could be skipped. For adjacency computation, we identify valid edges firstly. An edge is considered invalid if the two adjacent primitives are smoothly connected along the edge. Searching valid edges is accomplished by OCCT. Next, we compute the distance from each point to all valid edges. A point is marked as near an edge if the minimum distance is below a threshold (set to $0.08 \times ShapeArea/4\pi$ in this paper). For the primitive type and main axis direction of a point, we first determine which primitive it attached, OCCT is then used to analyze the primitive, providing both the primitive type and main axis direction.

In the absence of B-Rep data, such as working with mesh or voxel models, it can be converted to point cloud, after which the CstPnt module can be used to predict constraints. Since each point's constraints are local information, the computation only requires data from its neighboring points, meaning that global information is unnecessary. The constraint computation of a point p could be divided into the following steps: **Step 1:** Identify neighbor points around p . **Step 2:** From all neighbor points, identify which belongs to the same primitive as p , store in P_{valid} . **Step 3:** Fit shapes such as cylinders or planes using P_{valid} , and determine the primitive type with the smallest fitting error. **Step 4:** Based on P_{valid} and the primitive type, calculate the main axis direction and assess whether the point is near an edge. While the above process can be carried out using traditional methods, it is highly complex, which is why a deep learning model is employed to achieve the same.

The design of CstPnt module is inspired by the above steps, with details in Fig. 7. For **Step 1**, the traditional approach is to use the k-Nearest Neighbors (KNN) algorithm, which identifies neighbors within a sphere. However, for

constraint computation, it is more effective to search for neighbors along the shape’s surface. This approach captures more relevant points while reducing the influence of redundant points, as shown in Fig. 6. To this end, we proposed a neighbor searching method called SurfaceKNN, details in supplementary. For **Step 2**, the attention mechanism between points is employed to approximate this process, which applies different weights to neighbor points when updating the center point’s embedding, the relation between points is designed as embedding subtraction, as shown in Eq. (1). **Step 3** and **Step 4** involve computing MAD and PT, both steps can be accomplished by MLPs. We employed a U-Net-like structure for better data utilization.

$$\mathbf{f}'_i = \sum_{\mathbf{f}_j \in \mathcal{N}_i} \rho \left(\text{MLP}(\mathbf{Q}(\mathbf{f}_i) - \mathbf{K}(\mathbf{f}_j)) \right) \odot \mathbf{V}(\mathbf{f}_i). \quad (1)$$

Where \mathcal{N}_i is the feature collection of all neighbor points around \mathbf{p}_i , ρ is the normalization function (softmax in this paper), and \odot denotes element-wise multiplication. $\mathbf{Q}(\mathbf{f})$, $\mathbf{K}(\mathbf{f})$, and $\mathbf{V}(\mathbf{f})$ are defined in similar structure by concatenating \mathbf{f} with the positional encoding Δ , and then feeding it into MLPs, where Δ is defined as $\Delta = \mathbf{p}_i - \mathbf{p}_j$.

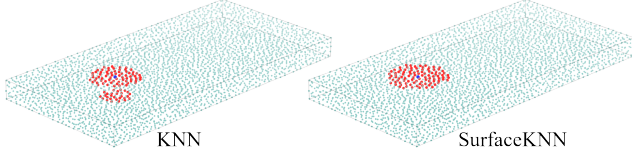


Figure 6. **Comparison of KNN and SurfaceKNN.** Blue point: center of neighbor search, red point: searched neighbors.

The structure of CstPnt reveals that only local information is utilized, which aligns with the local nature of the constraint representation we designed. For no global information is incorporated and most CAD shapes consist of a limited set of primitives, such as plane, cylinder, and sphere, the CstPnt could generalize to unseen datasets if pre-trained on a large scale dataset. The training data is derived from unlabeled B-Rep data, as a result, our CstPnt enables the effective use of existing large scale unlabeled B-Rep datasets, making it possible to serve meaningful tasks.

3.4. Constraint-Aware Feature Learning

The Stage 2 of CstNet is designed to leverage constraints effectively, which extracts features from MAD, Adj, PT separately, and attention between features is then applied to update constraint feature, with details in Fig. 7.

The Triple MLP takes the coordinates, MAD, Adj, and PT as inputs. In this module, the coordinates are concatenated with three constraint components separately, and then feeds into three individual MLPs. The outputs are the Axis

Feature, Adjacency Feature, and Primitive Feature, respectively. In the C-MLP layer, coordinates are concatenated with MAD, Adj, PT, and then feeds into MLPs, with the output being the initial Parametric Feature. The Quartic SSA layer takes the Axis Feature, Adjacency Feature, Primitive Feature, and Parametric Feature as input. This layer consists of four paths, each processing the corresponding feature independently. In each path, Farthest Point Sampling (FPS) is performed to reduce the point scale. Subsequently, SurfaceKNN is used to search for neighbors of each sampled point. The outputs of FPS and SurfaceKNN are shared across the four paths. Finally, the point-level attention layers are employed to update the sample points’ feature by its neighbors. The point-level attention here with a slight modification in the positional encoding Δ compare with Eq. (1). For the path takes XYZ & MAD as input, $\Delta = [(\mathbf{p}_i - \mathbf{p}_j) \| (\mathbf{n}_i - \mathbf{n}_j)]$, where $\mathbf{n}_i, \mathbf{n}_j$ represents the MAD of \mathbf{p}_i and \mathbf{p}_j . For the paths that use XYZ & (Adj or PT) as input, $\Delta = [(\mathbf{p}_i - \mathbf{p}_j) \| \mathbf{a}_i \| \mathbf{a}_j]$, where $\mathbf{a}_i, \mathbf{a}_j$ is the one-hot encoding of Adj or PT, $[\cdot \| \cdot]$ indicates concatenation in feature channel. Through Sampling, neighbor Searching, and Attention (SSA), the point cloud is down-scaled and features are updated. The Fea Attention layer also takes the Axis Feature, Adjacency Feature, Primitive Feature, and Parametric Feature as input, feature-level attention is employed to update the constraint feature efficiently. This design considers that different points may focus on different features, for example, points near edge may focus more on the Adjacency Feature, while others may pay more attention to the Primitive or Axis Feature. The Fea Attention is developed by vector attention as formulated in Eq. (2).

$$\mathbf{f}'_{\text{cst}} = \sum_{\mathbf{f}_j \in \mathcal{F}} \rho \left(\text{MLP}(\mathbf{Q}(\mathbf{f}_{\text{cst}}) - \mathbf{K}(\mathbf{f}_j)) \right) \odot \mathbf{V}(\mathbf{f}_{\text{cst}}). \quad (2)$$

In which $\mathcal{F} = \{\mathbf{f}_{\text{mad}}, \mathbf{f}_{\text{adj}}, \mathbf{f}_{\text{pt}}, \mathbf{f}_{\text{cst}}\}$, corresponding to Axis Feature, Adjacency Feature, Primitive Feature, and Constraint Feature. Δ is the one-hot encoding of \mathbf{f}_j type.

For downstream classification tasks, the constraint features obtained in each module will be concatenated by residual connection and feed into maxpooling, MLPs and softmax. Constraint features obtained by different modules may differ in features’ number and channel, based on the coordinates of the final constraint features, we identify the correspondence from different modules for further processing.

4. Experiments

4.1. Experimental Settings

We train CstNet using the Negative Log Likelihood Loss and optimized by Adam optimization for 200 epochs, with a weight decay of 0.0001 and an initial learning rate of 0.0001. We use StepLR learning rate scheduler, with step

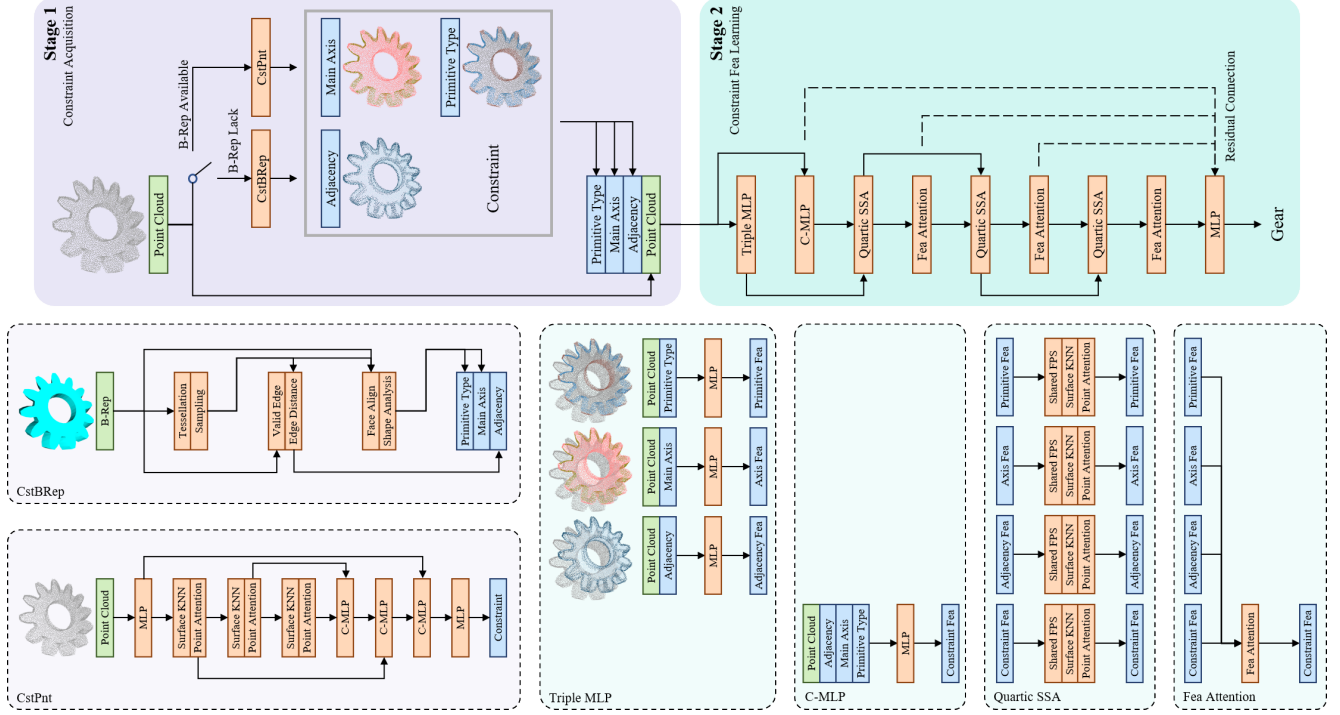


Figure 7. **Overview of CstNet.** The top side illustrates the overall architecture of CstNet, which comprising two stages. Stage 1 is designed for constraint acquisition. When B-Rep data is available, the CstBRep module is utilized to extract constraints; otherwise, use the CstPnt module. Stage 2 performs constraint feature learning, facilitating a deeper understanding of CAD shapes. The bottom side presents the details of module design. In the CstPnt module, the final MLP consists of three parallel MLPs with the same input, where the outputs correspond to Main Axis Direction, Adjacency, and Primitive Type.

size of 20 and gamma of 0.7. The batch size is 16. All experiments are performed on GeForce RTX 4090 GPU.

Param20K dataset Param20K contains 19,739 multi-modal instances categorized into 75 classes. Each instance includes B-Rep data, mesh, and point cloud. All B-Rep data are collected from the following three sources. More details in the supplementary. **Sources 1** (36.05 %): Downloaded and purified from TraceParts [18]. The CAD shapes on TraceParts are collected from manufacturing companies. **Sources 2** (24.12 %): Provided by a CAD company¹ that collaborates with our team. These shapes are all mechanical components. **Sources 3** (39.83 %): Instantiated from parametric templates designed by our team. These templates are designed based on common mechanical structures.

Our Param20K dataset encompasses various common formats of CAD shapes, making it suitable for a wide range of tasks. The careful selection and purification process undertaken by our team further ensures its high quality.

4.2. Constraint Acquisition

The extraction of constraints from B-Rep data is accomplished by the CstBRep module, with results visualized in

the Ground Truth column of Fig. 8. By referring to the model row, CstBRep performs well in extracting MAD, Adj, and PT from B-Rep data. Predicting MAD, Adj, and PT from point cloud is achieved by the CstPnt module. The training set is sourced from 25 trunks of ABC [20], with each trunk containing 10,000 B-Rep files. We utilized CstBRep module to extract constraints as Ground Truth for model training. After the training finished, the MSE loss of MAD is 0.0559, the prediction accuracy of Adj and PT reached 94.62% and 94.23%, respectively. In subsequent experiments, the above pre-trained CstPnt module is utilized to predict MAD, Adj, and PT with its weights frozen and no further updates. To ensure that only point cloud is used as input across all methods when comparing, even when B-Rep data is available, the CstBRep module will not be activated to obtain MAD, Adj, and PT.

After CstPnt was pre-trained, we evaluated it on a ABC new trunk and Param20K dataset. The ABC new trunk was treated as the test set, while the Param20K was considered as an unseen CAD shapes dataset, more results on other public available CAD shapes datasets in supplementary. Since there is no existing model that directly predicts MAD, Adj, and PT, we modified the published CAD-specific methods [41, 58] by adding MLPs as prediction head to en-

¹<https://www.newdimchina.com/>

able these predictions. The experiment results are shown in Tab. 1, from which our CstPnt achieves the highest accuracy in predicting MAD, Adj, and PT. Furthermore, from ABC to Param20K, all methods’ performance decreased, but our method dropped least accuracy. ParSeNet and HPNet may be negatively affected by global features, which impaired their performance on unseen datasets. Fig. 8 presents the visualization of constraint prediction results, which shown that our method is closest to the ground truth. Furthermore, from ABC to Param20K, our method demonstrates excellent generalization performance on unseen datasets. In contrast, while ParSeNet and HPNet exhibit acceptable prediction results on the ABC new trunk, they performed unsatisfactory on the unseen Param20K dataset.

4.3. Classification

To validate the ability of our CstNet in identifying CAD shapes that are visual similar but different in constraints, we conducted experiments on the Prism-Cuboid datasets presented in the Problem Statement section Sec. 3.1. Results shown in Fig. 9, in which our CstNet achieved best instance accuracy in distinguish 50° to 87° prisms and cuboids, which demonstrate the strong ability of CstNet in recognizing shapes with similar appearance but constraints different. For the binary classification of 89° prisms and cuboids, all methods achieved approximately 50% instance accuracy, this is attributed to the differences between them are so subtle that no one is capable to distinguishing them.

The classification of prisms and cuboids is predominantly influenced by constraints, while the comprehension of common CAD shapes necessitates the integration of both constraint and geometric features. CstNet achieves this by concatenating XYZ with constraint in Stage 2, thereby integrating geometric features into constraint features. To evaluate CstNet’s performance on common CAD shapes, we conducted experiments on Param20K dataset (more results on public CAD shapes dataset in Supplementary), results are presented in Tab. 2, where our CstNet outperformed other methods across both metrics, validated the effective-

Table 1. **Constraint prediction on ABC (new trunk) and Param20K.** MAD: MSE loss of Main Axis Direction. Adj, PT: prediction accuracy of Adjacency and Primitive Type.

DataSet	Method	MAD↓	Adj↑	PT↑
ABC	ParSeNet [41]	0.1356	84.89	85.22
	HPNet [58]	0.1576	82.63	79.15
	Ours	0.0998	90.24	91.19
Param20K	ParSeNet [41]	0.2247	81.42	59.75
	HPNet [58]	0.2570	78.60	57.66
	Ours	0.1390	87.95	86.52

Table 2. **Classification results on Param20K dataset.** Acc: accuracy over instance %, Acc*: accuracy over class %, F1: F1-score, mAP: mean average precision %.

Method	Acc	Acc*	F1	mAP
PointCNN [27]	80.25	76.03	74.64	83.38
PointNet [36]	81.30	83.21	82.06	85.18
PointNet++ [37]	83.70	86.37	85.30	87.94
PointConv [51]	82.30	85.62	84.91	87.92
DGCNN [46]	85.40	87.28	86.43	89.17
3DGCN [29]	86.42	88.25	87.63	89.81
Ours	89.94	91.06	90.34	92.72

ness of utilizing constraint and geometric features.

To access the robustness of CstNet, we evaluated it under rotated point clouds. Since point clouds are pre-processed by aligning their centroids to the origin and scaling their ranges into a unit cube, the performance of all methods is unaffected by point cloud shifts and scaling. Comparison results depicted in Fig. 10, from which our CstNet demonstrates strongest robustness to point cloud rotation. The dashed line in Fig. 10 show that the performance of CstPnt module remains nearly unaffected by rotation, owing to it learned various local features from ABC dataset.

4.4. Ablation Studies

Our CstNet leverages all three components of constraint: MAD, Adj, and PT. Additionally, we utilized the SurfaceKNN to obtain more efficient neighbors for each point. To validate the effectiveness of our design, we conducted a series of ablation studies on Param20K dataset.

For each component of constraint, we evaluated their importance by disabling one or all at a time. This operation is performed by setting the disabled components as a zero tensor before feeding into CstNet. Classification results are presented in Tab. 3, which show that all three components contribute to improving the performance of our CstNet. To assess the effectiveness of SurfaceKNN, we compared it with KNN. From Tab. 3, it can be concluded that in most cases, our SurfaceKNN outperforms KNN. However, when the Primitive Type is disabled, the results are similar between the two methods, indicating that SurfaceKNN primarily enhances the effectiveness of the Primitive Feature.

To validate the effectiveness of Stage 2 backbone, we conducted a comprehensive evaluation by feeding (x, y, z, MAD, Adj, PT) into multiple classification backbone for comparison. The results are presented in Tab. 4, from which our method demonstrates best performance under both predicted and label constraints, indicating that our design achieves the best utilization of constraints. Furthermore, although the accuracy using predicted constraints is lower than that of using label constraints, it still shows a

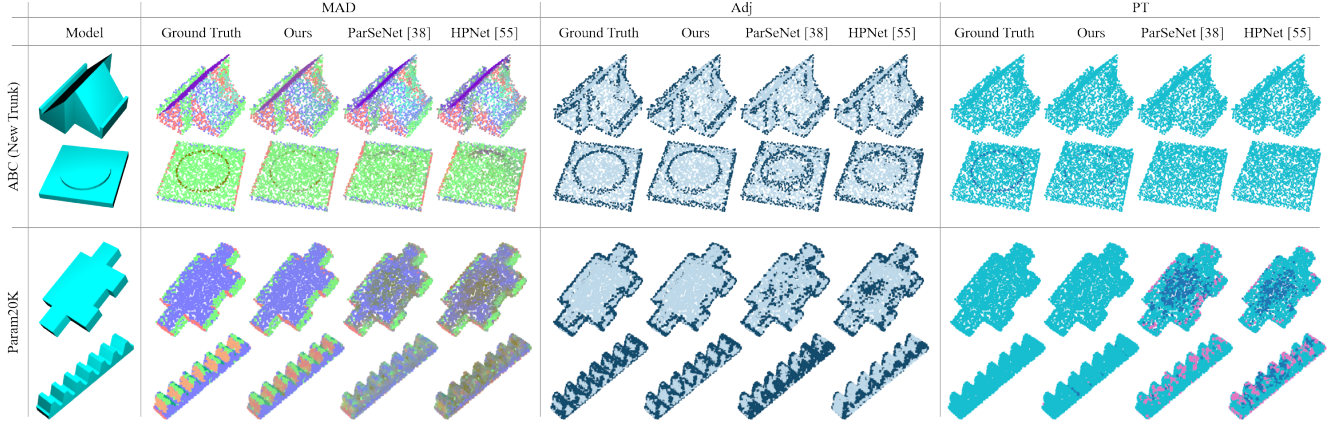


Figure 8. Constraint prediction visualization on ABC and Param20K. MAD is processed for visualization, details in supplementary.

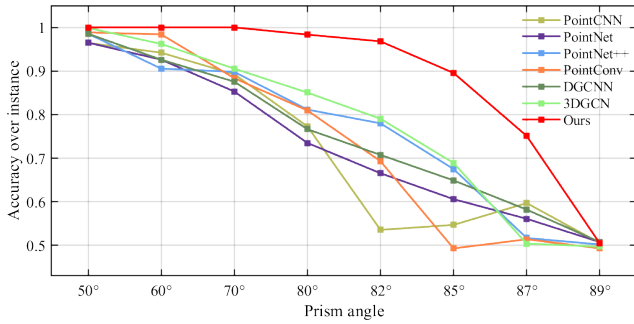


Figure 9. Classification results on Prism-Cuboid dataset.

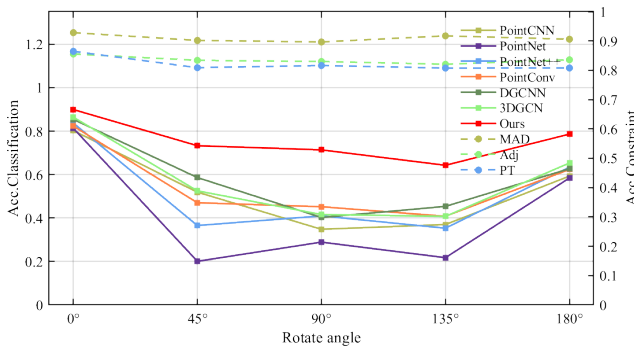


Figure 10. Classification results on rotated Param20K. The training set remained unchanged and the test set was rotated by a certain angle along the +Z direction. Solid line: left y axis, dashed line: right y axis. $\text{Acc.MAD} = 1 - \text{MAD.MSELoss}$.

significant improvement compared to the baselines without constraints. This highlights the effectiveness of the predicted constraints in improving model performance.

5. Conclusions

In this paper, we studied the constraints of CAD shapes and introduced its deep learning-friendly expression. Af-

Table 3. Effects on varying neighbor search and constraint components. Upper half: SurfaceKNN, lower half: KNN.

Constraint			Acc	Acc*	F1	mAP
MAD	Adj	PT				
✓	✓	✓	89.94	91.06	90.34	92.72
✗	✓	✓	86.32	89.05	88.38	90.59
✓	✗	✓	88.14	89.61	88.64	91.35
✓	✓	✗	88.68	88.94	89.01	91.22
✗	✗	✗	83.99	84.05	82.54	86.15
✓	✓	✓	89.03	90.00	89.22	91.43
✗	✓	✓	85.04	85.93	85.74	88.08
✓	✗	✓	87.27	88.23	87.98	90.00
✓	✓	✗	88.73	88.97	88.91	91.21
✗	✗	✗	83.19	82.54	81.46	86.34

Table 4. Effects on Stage2 Backbone. Upper half: predicted constraints from CstPnt, lower: label constraints.

Backbone-S2	Acc	Acc*	F1	mAP
PointNet [36]	83.83	83.64	83.20	87.27
PointNet++ [37]	85.52	88.11	87.18	90.79
DGCNN [46]	86.81	88.70	87.70	91.35
3DGCN [29]	87.46	89.59	87.97	91.92
Ours	89.94	91.06	90.34	92.72
PointNet [36]	86.24	85.99	86.33	91.00
PointNet++ [37]	86.60	88.82	87.71	90.74
DGCNN [46]	87.72	89.14	88.78	91.16
3DGCN [29]	89.29	89.81	89.00	92.62
Ours	91.80	92.52	91.76	94.20

terward, we proposed the CstNet for extracting and leveraging constraints. Additionally, we built up a multi-modal

CAD shape dataset Param20K. Extensive experiment results demonstrate that our CstNet achieves state-of-the-art performance on both accuracy and robustness. Comprehensive ablation studies further validate the effectiveness of constraints, SurfaceKNN, and network backbone.

CAD shapes possess numerous attributes. In this paper, we analyze the constraints from a functional perspective. In future work, we plan to investigate additional aspects such as part design and manufacturing procedure, to achieve a deeper understanding of CAD shapes.

References

- [1] A. Angrish, B. Craver, and B. Starly. Fabsearch: A 3d cad model-based search engine for sourcing manufacturing services. *Journal of Computing and Information Science in Engineering*, 19(4), 2019. Export Date: 08 October 2024; Cited By: 23. [2](#)
- [2] M. Atzmon, H. Maron, and Y. Lipman. Point convolutional neural networks by extension operators. *ACM Transactions on Graphics*, 37(4), 2018. Export Date: 31 July 2024; Cited By: 222. [2](#)
- [3] Dieter Roller Beat Brüderlin, editor. *Geometric Constraint Solving and Applications*. Springer Berlin Heidelberg, 1998. [2](#)
- [4] D. Y. Chen, X. P. Tian, Y. T. Shen, and M. Ouhyoung. On visual similarity based 3d model retrieval. In *Computer Graphics Forum*, pages 223–232, 2003. Export Date: 28 June 2024; Cited By: 1323. [3](#)
- [5] Yan Chen, Di Huang, Zhichao Liao, Xi Cheng, Xinghui Li, and Lone Zeng. Training-free point cloud recognition based on geometric and semantic information fusion. *arXiv preprint arXiv:2409.04760*, 2024. [2](#)
- [6] E. Dupont, K. Cherenkova, A. Kacem, S. A. Ali, I. Arzhanikov, G. Gusev, and D. Aouada. Cadops-net: Jointly learning cad operation types and steps from boundary-representations. In *Proceedings - 2022 International Conference on 3D Vision, 3DV 2022*, pages 114–123, 2022. Export Date: 06 July 2024; Cited By: 2. [3](#)
- [7] Y. Feng, Z. Zhang, X. Zhao, R. Ji, and Y. Gao. Gvcnn: Group-view convolutional neural networks for 3d shape recognition. In *Proceedings of the IEEE Computer Society Conference on Computer Vision and Pattern Recognition*, pages 264–272, 2018. Export Date: 31 July 2024; Cited By: 502. [2](#)
- [8] Yaroslav Ganin, Sergey Bartunov, Yujia Li, Ethan Keller, and Stefano Saliceti. Computer-aided design as language. *Advances in Neural Information Processing Systems*, 34:5885–5897, 2021. [2](#)
- [9] A. Goyal, H. Law, B. Liu, A. Newell, and J. Deng. Revisiting point cloud shape classification with a simple and effective baseline. In *Proceedings of Machine Learning Research*, pages 3809–3820, 2021. Export Date: 31 July 2024; Cited By: 92. [2](#)
- [10] H. Guo, S. Liu, H. Pan, Y. Liu, X. Tong, and B. Guo. Complexgen: Cad reconstruction by b-rep chain complex generation. *ACM Transactions on Graphics*, 41(4), 2022. Export Date: 23 July 2024; Cited By: 20. [3](#)
- [11] M. H. Guo, J. X. Cai, Z. N. Liu, T. J. Mu, R. R. Martin, and S. M. Hu. Pct: Point cloud transformer. *Computational Visual Media*, 7(2):187–199, 2021. Export Date: 31 July 2024; Cited By: 917. [2](#)
- [12] Q. Huang, W. Wang, and U. Neumann. Recurrent slice networks for 3d segmentation of point clouds. In *Proceedings of the IEEE Computer Society Conference on Computer Vision and Pattern Recognition*, pages 2626–2635, 2018. Export Date: 31 July 2024; Cited By: 391. [2](#)
- [13] F. Hähnlein, C. Li, N. J. Mitra, and A. Bousseau. Cad2sketch. *ACM Transactions on Graphics*, 41(6), 2022. Export Date: 23 July 2024; Cited By: 1. [3](#)
- [14] S. Jayanti, Y. Kalyanaraman, N. Iyer, and K. Ramani. Developing an engineering shape benchmark for cad models. *CAD Computer Aided Design*, 38(9):939–953, 2006. Export Date: 08 October 2024; Cited By: 280. [2](#)
- [15] P. K. Jayaraman, A. Sanghi, J. G. Lambourne, K. D. D. Willis, T. Davies, H. Shayani, and N. Morris. Uv-net: Learning from boundary representations. In *Proceedings of the IEEE Computer Society Conference on Computer Vision and Pattern Recognition*, pages 11698–11707, 2021. Export Date: 28 June 2024; Cited By: 27. [3](#)
- [16] Benjamin Jones, Dalton Hildreth, Duowen Chen, Ilya Baran, Vladimir G. Kim, and Adriana Schulz. Automate: a dataset and learning approach for automatic mating of cad assemblies. *ACM Transactions on Graphics*, 40(6):1–18, 2021. [3](#)
- [17] E. Kalogerakis, M. Averkiou, S. Maji, and S. Chaudhuri. 3d shape segmentation with projective convolutional networks. In *Proceedings - 30th IEEE Conference on Computer Vision and Pattern Recognition, CVPR 2017*, pages 6630–6639, 2017. Export Date: 31 July 2024; Cited By: 256. [2](#)
- [18] S. Kim, H. G. Chi, X. Hu, Q. Huang, and K. Ramani. A large-scale annotated mechanical components benchmark for classification and retrieval tasks with deep neural networks. In *Lecture Notes in Computer Science (including subseries Lecture Notes in Artificial Intelligence and Lecture Notes in Bioinformatics)*, pages 175–191, 2020. Export Date: 07 October 2024; Cited By: 33. [6](#), [2](#)
- [19] R. Klokov and V. Lempitsky. Escape from cells: Deep kd-networks for the recognition of 3d point cloud models. In *Proceedings of the IEEE International Conference on Computer Vision*, pages 863–872, 2017. Export Date: 31 July 2024; Cited By: 857. [2](#)
- [20] S. Koch, A. Matveev, Z. Jiang, F. Williams, A. Artemov, E. Burnaev, M. Alexa, D. Zorin, and D. Panozzo. Abc: A big cad model dataset for geometric deep learning. In *Proceedings of the IEEE Computer Society Conference on Computer Vision and Pattern Recognition*, pages 9593–9603, 2019. Export Date: 08 October 2024; Cited By: 279. [2](#), [6](#)
- [21] J. G. Lambourne, K. D. D. Willis, P. K. Jayaraman, A. Sanghi, P. Meltzer, and H. Shayani. Brepnet: A topological message passing system for solid models. In *Proceedings of the IEEE Computer Society Conference on Computer Vision and Pattern Recognition*, pages 12768–12777, 2021. Export Date: 28 June 2024; Cited By: 31. [3](#), [2](#)

- [22] T. Le and Y. Duan. Pointgrid: A deep network for 3d shape understanding. In *Proceedings of the IEEE Computer Society Conference on Computer Vision and Pattern Recognition*, pages 9204–9214, 2018. Export Date: 31 July 2024; Cited By: 324. [2](#)
- [23] C. Li, H. Pan, A. Bousseau, and N. J. Mitra. Sketch2cad: Sequential cad modeling by sketching in context. *ACM Transactions on Graphics*, 39(6), 2020. Export Date: 23 July 2024; Cited By: 42. [3](#)
- [24] C. Li, H. Pan, A. Bousseau, and N. J. Mitra. Free2cad: Parsing freehand drawings into cad commands. *ACM Transactions on Graphics*, 41(4), 2022. Export Date: 23 July 2024; Cited By: 27. [3](#)
- [25] Hongwei Li. *Poisson disk sampling: modern techniques*. Thesis, The Hong Kong University of Science and Technology Library, 2010. [4](#)
- [26] Lingxiao Li, Minhuyk Sung, Anastasia Dubrovina, Li Yi, and Leonidas J. Guibas. Supervised fitting of geometric primitives to 3d point clouds. In *2019 IEEE/CVF Conference on Computer Vision and Pattern Recognition (CVPR)*, page 2647–2655. IEEE, 2019. [1](#), [2](#)
- [27] Y. Li, R. Bu, M. Sun, W. Wu, X. Di, and B. Chen. Pointcnn: Convolution on x-transformed points. In *Advances in Neural Information Processing Systems*, pages 820–830, 2018. Export Date: 08 October 2024; Cited By: 1859. [2](#), [7](#), [3](#)
- [28] Zhichao Liao, Di Huang, Heming Fang, Yue Ma, Fengyuan Piao, Xinghui Li, Long Zeng, and Pingfa Feng. Free-hand sketch generation from mechanical components. *arXiv preprint arXiv:2408.05966*, 2024. [3](#)
- [29] Z. H. Lin, S. Y. Huang, and Y. C. F. Wang. Learning of 3d graph convolution networks for point cloud analysis. *IEEE Transactions on Pattern Analysis and Machine Intelligence*, 44(8):4212–4224, 2022. Export Date: 08 October 2024; Cited By: 35. [2](#), [7](#), [8](#), [3](#)
- [30] Y. Liu, B. Fan, S. Xiang, and C. Pan. Relation-shape convolutional neural network for point cloud analysis. In *Proceedings of the IEEE Computer Society Conference on Computer Vision and Pattern Recognition*, pages 8887–8896, 2019. Export Date: 31 July 2024; Cited By: 664.
- [31] X. Ma, C. Qin, H. You, H. Ran, and Y. Fu. Rethinking network design and local geometry in point cloud: A simple residual mlp framework. In *ICLR 2022 - 10th International Conference on Learning Representations*, 2022. Export Date: 31 July 2024; Cited By: 172. [2](#)
- [32] B. Manda, P. Bhaskare, and R. Muthuganapathy. A convolutional neural network approach to the classification of engineering models. *IEEE Access*, 9:22711–22723, 2021. Export Date: 28 June 2024; Cited By: 18. [3](#)
- [33] D. Maturana and S. Scherer. Voxnet: A 3d convolutional neural network for real-time object recognition. In *IEEE International Conference on Intelligent Robots and Systems*, pages 922–928, 2015. Export Date: 31 July 2024; Cited By: 2809. [2](#)
- [34] W. R. Para, S. F. Bhat, P. Guerrero, T. Kelly, N. Mitra, L. Guibas, and P. Wonka. Sketchgen: Generating constrained cad sketches. In *Advances in Neural Information Processing Systems*, pages 5077–5088, 2021. Export Date: 07 July 2024; Cited By: 23. [3](#)
- [35] Janusz Pobożniak. Algorithm for iso 14649 (step-nc) feature recognition. *Management and Production Engineering Review*, 4(4):50–58, 2013. [1](#)
- [36] C. R. Qi, H. Su, K. Mo, and L. J. Guibas. Pointnet: Deep learning on point sets for 3d classification and segmentation. In *Proceedings - 30th IEEE Conference on Computer Vision and Pattern Recognition, CVPR 2017*, pages 77–85, 2017. Export Date: 31 July 2024; Cited By: 9040. [2](#), [7](#), [8](#), [3](#)
- [37] C. R. Qi, L. Yi, H. Su, and L. J. Guibas. Pointnet++: Deep hierarchical feature learning on point sets in a metric space. In *Advances in Neural Information Processing Systems*, pages 5100–5109, 2017. Export Date: 31 July 2024; Cited By: 6263. [7](#), [8](#), [2](#), [3](#)
- [38] S. Qiu, S. Anwar, and N. Barnes. Geometric back-projection network for point cloud classification. *IEEE Transactions on Multimedia*, 24:1943–1955, 2022. Export Date: 31 July 2024; Cited By: 110. [2](#)
- [39] G. Riegler, A. O. Ulusoy, and A. Geiger. Octnet: Learning deep 3d representations at high resolutions. In *Proceedings - 30th IEEE Conference on Computer Vision and Pattern Recognition, CVPR 2017*, pages 6620–6629, 2017. Export Date: 31 July 2024; Cited By: 1052. [2](#)
- [40] A. Seff, W. Zhou, N. Richardson, and R. P. Adams. Vitruvion: A generative model of parametric cad sketches. In *ICLR 2022 - 10th International Conference on Learning Representations*, 2022. Export Date: 07 July 2024; Cited By: 9. [2](#), [3](#)
- [41] Gopal Sharma, Difan Liu, Subhransu Maji, Evangelos Kalogerakis, Siddhartha Chaudhuri, and Radomír Měch. *ParSeNet: A Parametric Surface Fitting Network for 3D Point Clouds*, page 261–276. Springer International Publishing, 2020. [1](#), [2](#), [6](#), [7](#)
- [42] H. Su, S. Maji, E. Kalogerakis, and E. Learned-Miller. Multi-view convolutional neural networks for 3d shape recognition. In *Proceedings of the IEEE International Conference on Computer Vision*, pages 945–953, 2015. Export Date: 31 July 2024; Cited By: 2865. [2](#)
- [43] H. Thomas, C. R. Qi, J. E. Deschaud, B. Marcotegui, F. Goulette, and L. Guibas. Kpconv: Flexible and deformable convolution for point clouds. In *Proceedings of the IEEE International Conference on Computer Vision*, pages 6410–6419, 2019. Export Date: 31 July 2024; Cited By: 1705. [2](#)
- [44] M. A. Uy, Y. Y. Chang, M. Sung, P. Goel, J. Lambourne, T. Birdal, and L. Guibas. Point2cyl: Reverse engineering 3d objects from point clouds to extrusion cylinders. In *Proceedings of the IEEE Computer Society Conference on Computer Vision and Pattern Recognition*, pages 11840–11850, 2022. Export Date: 23 July 2024; Cited By: 17. [3](#)
- [45] P. S. Wang, Y. Liu, Y. X. Guo, C. Y. Sun, and X. Tong. O-cnn: Octree-based convolutional neural networks for 3d shape analysis. In *ACM Transactions on Graphics*, 2017. Export Date: 31 July 2024; Cited By: 851. [2](#)
- [46] Y. Wang, Y. Sun, Z. Liu, S. E. Sarma, M. M. Bronstein, and J. M. Solomon. Dynamic graph cnn for learning on point clouds. *ACM Transactions on Graphics*, 38(5), 2019. Export Date: 08 October 2024; Cited By: 3926. [2](#), [7](#), [8](#), [3](#)

- [47] X. Wei, R. Yu, and J. Sun. View-gcn: View-based graph convolutional network for 3d shape analysis. In *Proceedings of the IEEE Computer Society Conference on Computer Vision and Pattern Recognition*, pages 1847–1856, 2020. Export Date: 31 July 2024; Cited By: 197. [2](#)
- [48] Karl D.D. Willis, Pradeep Kumar Jayaraman, Hang Chu, Yunsheng Tian, Yifei Li, Daniele Grandi, Aditya Sanghi, Linh Tran, Joseph G. Lambourne, Armando Solar-Lezama, and Wojciech Matusik. Joinable: Learning bottom-up assembly of parametric cad joints. In *2022 IEEE/CVF Conference on Computer Vision and Pattern Recognition (CVPR)*. IEEE, 2022. [3](#)
- [49] K. D. D. Willis, P. K. Jayaraman, J. G. Lambourne, H. Chu, and Y. Pu. Engineering sketch generation for computer-aided design. In *IEEE Computer Society Conference on Computer Vision and Pattern Recognition Workshops*, pages 2105–2114, 2021. Export Date: 07 July 2024; Cited By: 30. [3](#)
- [50] R. Wu, C. Xiao, and C. Zheng. Deepcad: A deep generative network for computer-aided design models. In *Proceedings of the IEEE International Conference on Computer Vision*, pages 6752–6762, 2021. Export Date: 23 July 2024; Cited By: 47. [3](#)
- [51] W. Wu, Z. Qi, and L. Fuxin. Pointconv: Deep convolutional networks on 3d point clouds. In *Proceedings of the IEEE Computer Society Conference on Computer Vision and Pattern Recognition*, pages 9613–9622, 2019. Export Date: 09 October 2024; Cited By: 1264. [2](#), [7](#), [3](#)
- [52] Z. Wu, S. Song, A. Khosla, F. Yu, L. Zhang, X. Tang, and J. Xiao. 3d shapenets: A deep representation for volumetric shapes. In *Proceedings of the IEEE Computer Society Conference on Computer Vision and Pattern Recognition*, pages 1912–1920, 2015. Export Date: 31 July 2024; Cited By: 4378. [2](#)
- [53] T. Xiang, C. Zhang, Y. Song, J. Yu, and W. Cai. Walk in the cloud: Learning curves for point clouds shape analysis. In *Proceedings of the IEEE International Conference on Computer Vision*, pages 895–904, 2021. Export Date: 31 July 2024; Cited By: 130. [2](#)
- [54] M. Xu, R. Ding, H. Zhao, and X. Qi. Paconv: Position adaptive convolution with dynamic kernel assembling on point clouds. In *Proceedings of the IEEE Computer Society Conference on Computer Vision and Pattern Recognition*, pages 3172–3181, 2021. Export Date: 31 July 2024; Cited By: 272.
- [55] M. Xu, J. Zhang, Z. Zhou, M. Xu, X. Qi, and Y. Qiao. Learning geometry-disentangled representation for complementary understanding of 3d object point cloud. In *35th AAAI Conference on Artificial Intelligence, AAAI 2021*, pages 3056–3064, 2021. Export Date: 31 July 2024; Cited By: 58. [2](#)
- [56] X. Xu, K. D. D. Willis, J. G. Lambourne, C. Y. Cheng, P. K. Jayaraman, and Y. Furukawa. Skexgen: Autoregressive generation of cad construction sequences with disentangled codebooks. In *Proceedings of Machine Learning Research*, pages 24698–24724, 2022. Export Date: 23 July 2024; Cited By: 15. [3](#)
- [57] Y. Xu, T. Fan, M. Xu, L. Zeng, and Y. Qiao. Spidercnn: Deep learning on point sets with parameterized convolutional filters. In *Lecture Notes in Computer Science (including sub-series Lecture Notes in Artificial Intelligence and Lecture Notes in Bioinformatics)*, pages 90–105, 2018. Export Date: 08 October 2024; Cited By: 139. [2](#), [3](#)
- [58] Siming Yan, Zhenpei Yang, Chongyang Ma, Haibin Huang, Etienne Vouga, and Qixing Huang. Hpnet: Deep primitive segmentation using hybrid representations. In *2021 IEEE/CVF International Conference on Computer Vision (ICCV)*, page 2733–2742. IEEE, 2021. [1](#), [2](#), [6](#), [7](#)
- [59] Z. Yang and L. Wang. Learning relationships for multi-view 3d object recognition. In *Proceedings of the IEEE International Conference on Computer Vision*, pages 7504–7513, 2019. Export Date: 31 July 2024; Cited By: 125. [2](#)
- [60] T. Yu, J. Meng, and J. Yuan. Multi-view harmonized bilinear network for 3d object recognition. In *Proceedings of the IEEE Computer Society Conference on Computer Vision and Pattern Recognition*, pages 186–194, 2018. Export Date: 31 July 2024; Cited By: 240. [2](#)
- [61] Long Zeng, Yong-Jin Liu, Sang Hun Lee, and Matthew Ming-Fai Yuen. Q-complex: Efficient non-manifold boundary representation with inclusion topology. *Computer-Aided Design*, 44(11):1115–1126, 2012. [2](#)
- [62] Long Zeng, Zhi-kai Dong, Jia-yi Yu, Jun Hong, and Hong-yu Wang. Sketch-based retrieval and instantiation of parametric parts. *Computer-Aided Design*, 113:82–95, 2019. [1](#), [3](#)
- [63] Long Zeng, Wei Jie Lv, Xin Yu Zhang, and Yong Jin Liu. Parametricnet: 6dof pose estimation network for parametric shapes in stacked scenarios. In *2021 IEEE International Conference on Robotics and Automation (ICRA)*, page 772–778. IEEE, 2021. [2](#)
- [64] Z. Zhang, B. S. Hua, and S. K. Yeung. Shellnet: Efficient point cloud convolutional neural networks using concentric shells statistics. In *Proceedings of the IEEE International Conference on Computer Vision*, pages 1607–1616, 2019. Export Date: 31 July 2024; Cited By: 313. [2](#)
- [65] Zaiwei Zhang, Bo Sun, Haitao Yang, and Qixing Huang. *H3DNet: 3D Object Detection Using Hybrid Geometric Primitives*, page 311–329. Springer International Publishing, 2020. [1](#), [2](#)
- [66] H. Zhao, L. Jiang, J. Jia, P. Torr, and V. Koltun. Point transformer. In *Proceedings of the IEEE International Conference on Computer Vision*, pages 16239–16248, 2021. Export Date: 31 July 2024; Cited By: 927. [2](#)
- [67] S. Zhou, T. Tang, and B. Zhou. Cadparser: A learning approach of sequence modeling for b-rep cad. In *IJCAI International Joint Conference on Artificial Intelligence*, pages 1804–1812, 2023. Export Date: 23 July 2024; Cited By: 0. [3](#)

Constraint-Aware Feature Learning for Parametric Point Cloud

Supplementary Material

F. Overview

This supplementary material provides additional details that supplement the main paper and includes more experimental results.

In Sec. G, we present the details of network architecture and data preparation in validation experiments. In Sec. H, we provide the data construction and static of Param20K dataset. Finally, Sec. I offers data process for visualization and more results of constraint acquisition and classification experiments. In Sec. J, we show more details of our constraint representation and constraint learning methods.

G. Validation Experiment

G.1. Constraint Expression

This section introduces the constraint expression in the validation experiments.

The constraint expression in validation experiments is defined in a simple manner: for a point, its constraint is defined by the relationship between the plane it attached and the reference plane, as shown in Fig. 11. This calculation process is carried out by openCASCADE Technology (OCCT). The constraint is represented in a one-hot encoding, where $(1, 0, 0)$ indicates perpendicular, $(0, 1, 0)$ indicates parallel, and $(0, 0, 1)$ indicates other constraints. Each point in the point cloud is expressed as $(Coordinate, constraint)$. For example, if the coordinate of a point is $(0.1, 0.2, 0.3)$, and the plane it attached is perpendicular to the reference plane, it is expressed as $(0.1, 0.2, 0.3, 1, 0, 0)$, where $(0.1, 0.2, 0.3)$ represents the point's coordinate, and $(1, 0, 0)$ denotes the type of constraint.

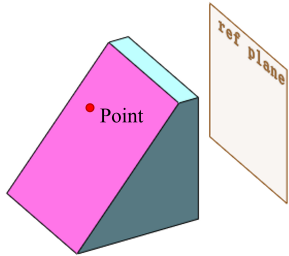


Figure 11. **Constraint expression in validation experiments.** The red point's constraint is expressed as the constraint type between the magenta plane and the reference plane, using one-hot encoding.

G.2. Dataset Generation

This section introduces the dataset generation procedures in the validation experiments.

The dataset generation for the validation experiments consists of the following steps:

1. Building the parametric templates for cuboids and prisms (with angles of $50^\circ, 60^\circ, 70^\circ, 80^\circ, 82^\circ, 85^\circ, 87^\circ, 89^\circ$). Afterwards determining the dimension range for each parameter. The parametric templates and the dimensions are shown in Fig. 12.
2. Assigning random values to the parameters in parametric templates. Each parametric template is instantiated into 5,000 B-Rep format CAD shapes, which are stored in STEP files [35].
3. Using OCCT to read the STEP files and convert them into meshes. Poisson disk sampling is then applied to sample points from meshes.
4. For the sampled points, OCCT is used to calculate the plane to which each point is attached. The constraint type for each point is then determined based on the relationship between the attached plane and the reference plane.
5. Rotating the generated point clouds randomly along the XYZ axes, within a range of $[-25^\circ, 25^\circ]$.
6. Assigning the generated point clouds to each experiments. The validation experiments involve binary classification of cuboids and prisms with specific angles. The point clouds used in each of the eight experiments are as follows (80 % for training, and 20 % for testing):

- Experiment 1: Cuboid \times 5000, Prism $50^\circ \times$ 5000
- Experiment 2: Cuboid \times 5000, Prism $60^\circ \times$ 5000
- Experiment 3: Cuboid \times 5000, Prism $70^\circ \times$ 5000
- Experiment 4: Cuboid \times 5000, Prism $80^\circ \times$ 5000
- Experiment 5: Cuboid \times 5000, Prism $82^\circ \times$ 5000
- Experiment 6: Cuboid \times 5000, Prism $85^\circ \times$ 5000
- Experiment 7: Cuboid \times 5000, Prism $87^\circ \times$ 5000
- Experiment 8: Cuboid \times 5000, Prism $89^\circ \times$ 5000

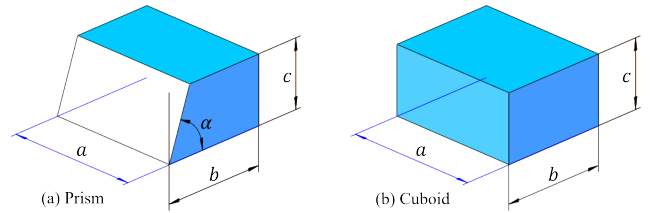


Figure 12. **Parametric templates for prisms and cuboids.** $a, b, c \in [0.3, 2.3]$, for prisms: $b > \frac{c}{\tan \alpha}$.

G.3. Model Design

This section introduces the structure of the constraint-aware model used in the validation experiments.

The constraint-aware model first employs a PointNet++ [37] backbone to predict point-wise constraints. These constraints are then concatenated with the point coordinates and passed through another PointNet++ backbone to determine the point cloud category. The model’s loss function is the sum of the classification loss and the constraint loss, as shown in Fig. 13

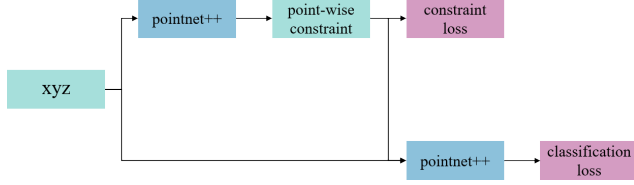


Figure 13. Constraint-aware model structure.

H. Param20K Dataset

H.1. Why build up the Param20K dataset?

The limited availability of B-Rep datasets poses barriers to deep learning on CAD shapes. Most existing CAD shape datasets consist of mesh files, such as MCB [18] and ESB [14]. While mesh files could approximate the appearance of CAD shapes, lack crucial boundary information. In contrast, B-Rep data [21, 61] serves as the native representation of CAD shapes and is therefore more suitable for dataset construction. However, labeled B-Rep datasets remain relatively scarce, for example, FabWave [1] includes only 2,133 B-Rep files. Although the ABC [20] contains a large number of B-Rep files, it remains unlabeled.

H.2. Dataset Construction

This section provide details of purification process and data acquisition of Param20K dataset.

Purification: The purification process involved removing broken, duplicated, or overly complex CAD shapes requiring more than 4,000 points for point cloud representation.

Point cloud: The point cloud data in Param20K dataset containing about 2,200 points, point constraints is also included, each point is expressed as (Coordinate, Primitive Type, Main Axis Direction, Adjacency), the meshes and point clouds are generated from B-Rep data.

H.3. Dataset Statics

This section presents the shapes count and proportion statistics for each category in the Param20K dataset. Additionally, shapes from each category are showcased.

Param20K dataset is divided into 80 % for training and 20 % for testing.

The class distribution is shown in Fig. 14.

The proportion of shapes in each category are shown in Fig. 15.

Shapes instantiated from the parametric templates designed by our team names begin with "Num".

Example shapes from each category are shown in Fig. 16.

I. Constraint Acquisition and Classification Experiments

I.1. Process to Visualize Main Axis Direction

The main axis direction of a point, denoted as $v = (x, y, z)$, is visualized as $R = \frac{x+1}{2}$, $G = \frac{y+1}{2}$, and $B = \frac{z+1}{2}$. Since the main axis direction is represented as a unit vector, $-1 \leq x, y, z \leq 1$, which results in $0 \leq \frac{x+1}{2}, \frac{y+1}{2}, \frac{z+1}{2} \leq 1$.

I.2. Constraint Visualization of CstBRep

More constraints extracted by the CstBRep module from the B-Rep are visualized in Fig. 17.

I.3. Constraint acquisition on MCB

We evaluated the pre-trained CstPnt module and ParSeNet [41], HPNet [58] on the CAD shape dataset MCB [18] to predict constraints. For the MCB consists of mesh files, it was not possible to extract Ground Truth constraints for comparison, therefore no ground truth presented in Fig. 18, and no numerical results are available. Based on the results visualized in Fig. 18, CstPnt demonstrated a high level of constraint prediction accuracy even on an unseen dataset.

I.4. Classification on MCB

We conducted evaluations on the CAD shape dataset MCB [18], with results presented in Tab. 5, from which our CstNet achieved the highest scores across all metrics, conclusions similar with experiments on Param20K dataset.

J. Constraint Learning Method Details

J.1. Defects of General Constraint Representation

The simple constraint expression in validation experiments is insufficient for a comprehensive definition, as selecting an appropriate reference plane for complex CAD shapes is challenging. Moreover, traditional constraint representations suffer from non-uniqueness, as shown in Fig. 19, defining the relations between three planes involves multiple constraint options, therefore, this approach is not well-suited for deep learning models.

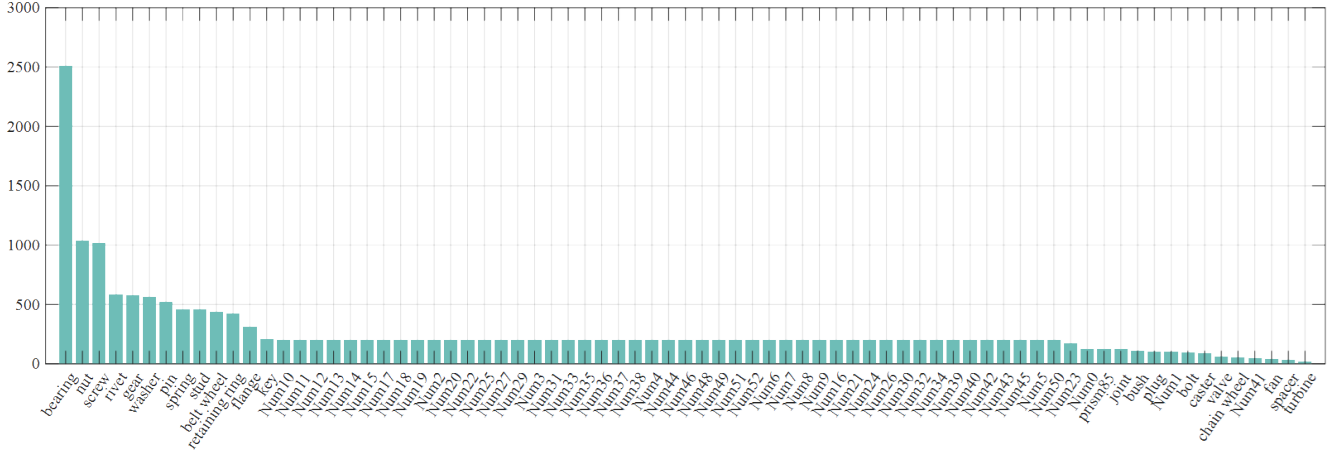


Figure 14. Quantity distribution of Param20K dataset.

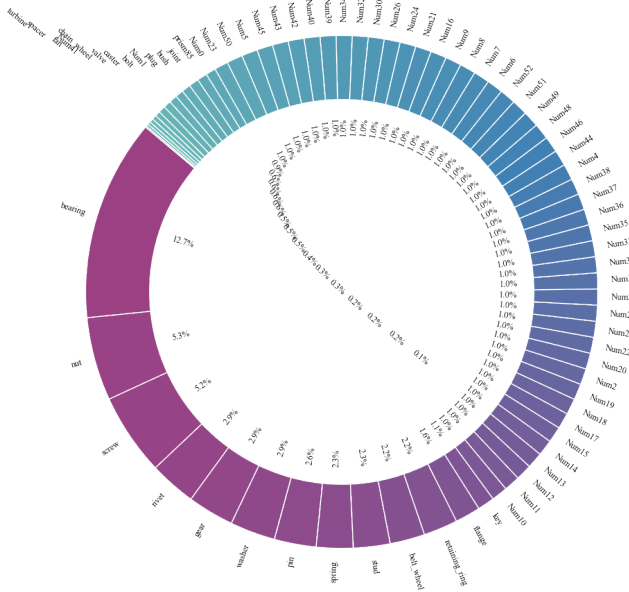


Figure 15. Shapes proportion of Param20K dataset.

The constraint is defined as a graph representation in some circumstances, where each node represents a primitive, and the edge between nodes represent their constraints. However, this approach is not well-suited for point cloud analysis. First, in cases where only point clouds are provided as input, the number of primitives is hard to obtain. Second, due to the unordered nature of point cloud, it is difficult to associate points with the corresponding primitives, making label design very challenging. Additionally, the graph representation essentially records the constraint relationships between each pair of primitives, for the CAD shapes contain many primitives, recording the relative positions between every pair of primitives would result in an overwhelming amount of data, making the expression of

Table 5. **Classification results on MCB.** Acc: accuracy over instance %, Acc*: accuracy over class %, F1: F1-score, mAP: mean average precision %.

Method	Acc	Acc*	F1	mAP
PointCNN [27]	93.89	81.85	83.86	90.13
PointNet [36]	86.78	67.70	86.55	74.08
PointNet++ [37]	87.45	73.68	88.32	91.33
SpiderCNN [57]	93.59	79.70	81.30	86.64
PointConv [51]	93.25	80.24	71.31	82.19
DGCNN [46]	92.54	74.47	76.12	74.27
3DGCN [29]	93.71	78.71	84.59	84.35
Ours	96.87	89.21	89.85	93.17

these relative positions impractical.

J.2. Unique Process of MAD

This section provides the process of Main Axis Direction and example constraint representation.

The main axis direction is processed to ensure its uniqueness, as one axis can determine two unit vectors with opposite direction. For a given axis, we first randomly select one of the two vectors, denoted as $v(x, y, z)$, and then process it using the following algorithm:

A point with constraint is expressed as Fig. 20.

J.3. CstBRep Module

This section explains why it is necessary to compute valid edges in the CstBRep module.

The CstBRep module is used to compute constraints from B-Rep data, and the computation process consists of the following steps:

Step 1: Point cloud generation (optional).

Step 2: Calculation of valid edges and the distance from each point to these valid edges. If the minimum distance

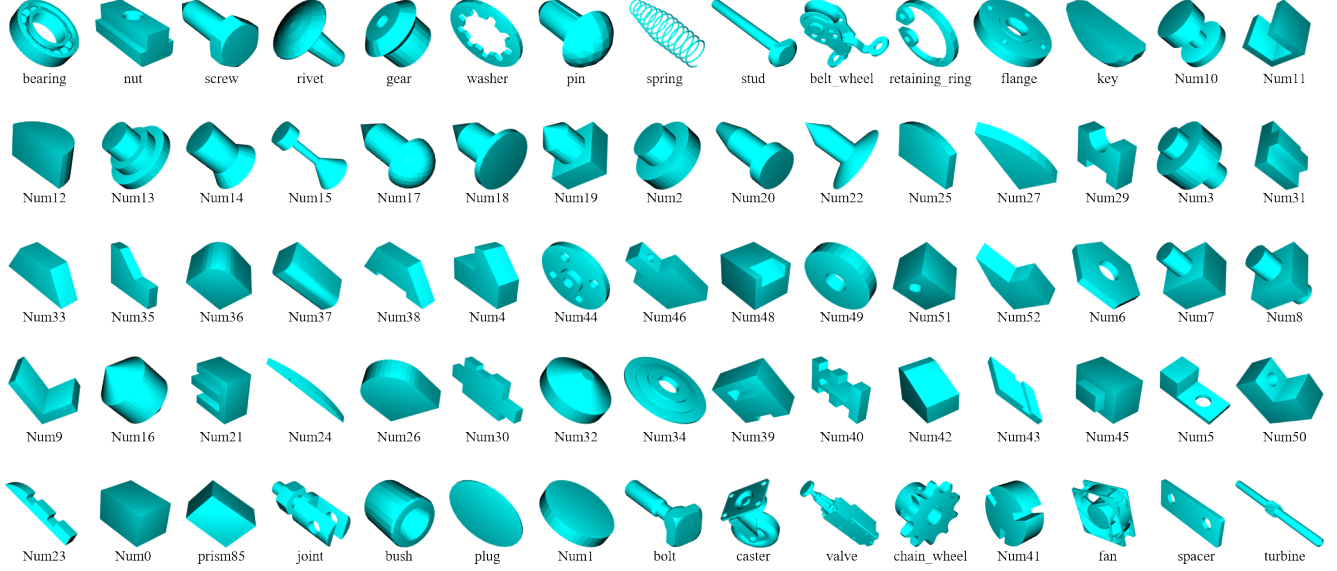


Figure 16. Example shapes for each category in Param20K dataset.

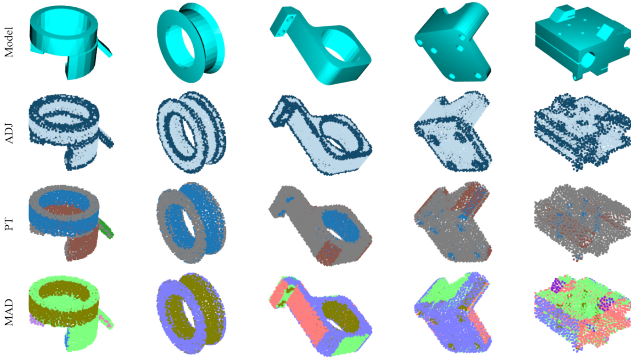


Figure 17. More constraint extraction results from the B-Rep data. ADJ: Adjacency, PMT: Primitive Type, MAD: Main Axis Direction.

is below a threshold, the point is classified as a edge-near point.

Step 3: Calculation of the primitives to which each point attached, followed by analysis to determine point’s Primitive Type and the Main Axis Direction.

In **Step 2**, valid edges are computed, as this helps to reduce the potential for data to mislead the deep learning model. The definition of valid edge is illustrated in Fig. 21. This definition is based on the observation that a complete cylinder in the B-Rep data stored in STEP files is often split into two half-cylinder faces. As a result, two generatrices form edges on the cylindrical surface, but the deep learning model cannot predict these edges, as shown in Fig. 22. Furthermore, in other cases, edges corresponding to smoothly connected faces are also difficult to identify, leading to confusion for deep learning models.

Data: Unit vector $v(x, y, z)$
Result: Unit vector after direction unification

```

1 if  $z < 0$  then
2    $v = -1 \times v$ ;
3   Return  $v$ ;
4 else if  $z == 0$  then
5   if  $y < 0$  then
6      $v = -1 \times v$ ;
7     Return  $v$ ;
8   else if  $y == 0$  then
9     if  $x < 0$  then
10       $v = -1 \times v$ ;
11      Return  $v$ ;
12 return  $v$ 

```

J.4. CstPnt Module

This section provides a detailed explanation of the valid points in the computational steps that inspire the design of the CstPnt Module.

The CstPnt Module is used to predict constraints from point clouds. The design of the CstPnt Module is inspired by the following calculation process:

For a point p in point cloud, its constraint could be calculated by the following steps:

1. Identify neighbor points around p .
2. From all neighbor points, identify those that belong to the same primitive as p ; these points are referred to as valid points.

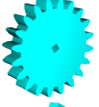
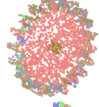
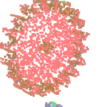
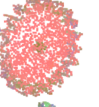
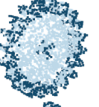
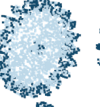

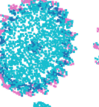




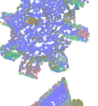
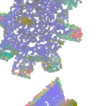






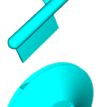
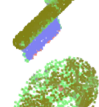
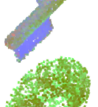
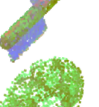






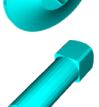







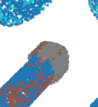


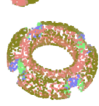






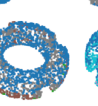














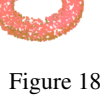

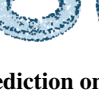




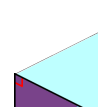

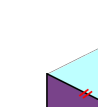
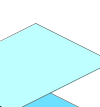


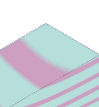



Model	MAD			Adj			PT		
	Ours	ParSeNet [7]	HPNet [11]	Ours	ParSeNet [7]	HPNet [11]	Ours	ParSeNet [7]	HPNet [11]
									
									
									
									
									
									
									
									

Figure 18. **Constraint prediction on MCB.**

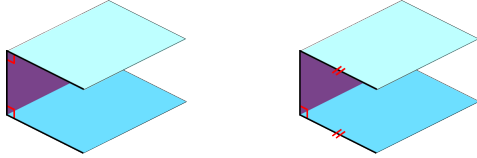


Figure 19. **Non-uniqueness of traditional constraint expression.** Left: Double vertical constraints, right: Vertical and parallel constraints.

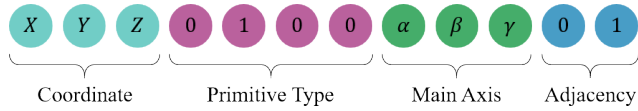


Figure 20. **Expression of a point with constraint.**

3. Fit shapes such as cylinders or planes using valid points, and determine the primitive type with the smallest fitting error.
4. Based on the valid points and the primitive type, calculate the main axis direction and assess whether the point is near an edge.

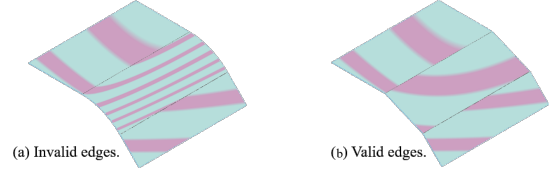


Figure 21. **Zebra stripes of primitives corresponding to invalid and valid edges.** Left: G1 or higher continuous at the invalid edges, right: G0 continuous at the valid edges.

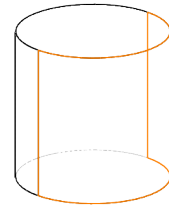


Figure 22. **Cylinder in B-Rep representation.** A complete cylindrical surface is represented as a combination of two half-cylinder surface, resulting in edges along the generatrices that cannot be recognized, thereby causing confusion for deep learning model.

In these steps, it is necessary to compute the valid points. We define the valid point as the neighbors that lie on the same primitive as the center point p , as visualized in Fig. 23. These valid points can be used to determine whether the center point is near an edge, as well as to calculate the main axis direction and primitive type of the attached primitive, while the invalid points do not contribute to these calculations.

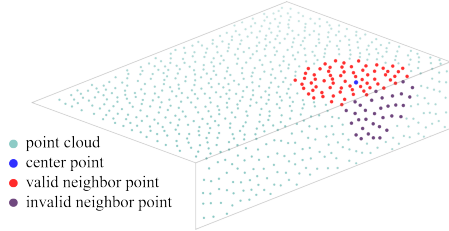


Figure 23. Valid and invalid points for constraint calculation.

J.5. SurfaceKNN

This section introduces the algorithm of SurfaceKNN.

SurfaceKNN based on the assumption that when KNN is applied with a small number of neighbors, the output points are searched along the shape's surface. This assumption has been validated in most cases. Leveraging this assumption, SurfaceKNN is accomplished by applying KNN with small number of neighbors iteratively. During each iteration, KNN is used to search a small set of neighboring points, which then serve as new central points for subsequent searches. This process continues until the desired number of points is obtained, as illustrated in Fig. 24.

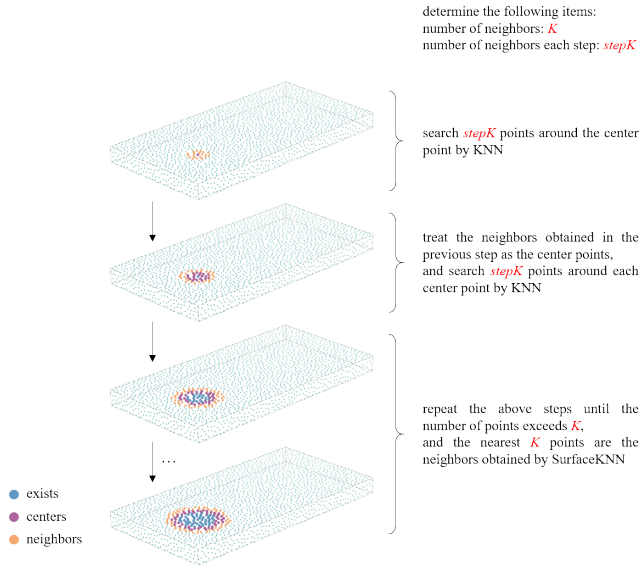


Figure 24. Algorithm of SurfaceKNN.